International Journal of Research in Medical Sciences
Brundavanam RK et al. Int J Res Med Sci. 2017 Jun;5(6):2454-2461
www.msjonline.org
pISSN 2320-6071 | eISSN 2320-6012
DOI: http://dx.doi.org/10.18203/2320-6012.ijrms20172428

Original Research Article

Synthesis of a bone like composite material derived from waste pearl oyster shells for potential bone tissue bioengineering applications

Ravi Krishna Brundavanam, Derek Fawcett, Gérrard Eddy Jai Poinern*

Department of Physics, Energy Studies and Nanotechnology, School of Engineering and Energy, Murdoch University, Murdoch, Western Australia 6150, Australia

Received: 20 March 2017
Accepted: 19 April 2017

***Correspondence:**
Dr. Gérrard Eddy Jai Poinern,
E-mail: g.poinern@murdoch.edu.au

ABSTRACT

Background: Hydroxyapatite is generally considered a viable substitute for bone in a number of medical procedures such as bone repair, bone augmentation and coating metal implants. Unfortunately, hydroxyapatite has poor mechanical properties that make it unsuitable for many load bearing applications.
Methods: In the present work various grades of finely crushed *Pinctada maxima* (pearl oyster shell) were combined with a nanometer scale hydroxyapatite powder to form novel composite materials. A comparative study was made between the various powder based composites synthesized. The crystalline structure and morphology of the various powder based composites were investigated using X-ray diffraction and field emission scanning electron microscopy. The composite materials were also evaluated and characterized.
Results: Manufactured hydroxyapatite powders were composed of crystalline spherical/granular particles with a mean size of 30 nm. Also produced were hydroxyapatite and finely crushed calcium carbonate from *Pinctada maxima* (pearl oyster shell) powder mixtures. Hydroxyapatite coatings produced on *Pinctada maxima* nacre substrates were investigated and their surface characteristics reported.
Conclusions: *Pinctada maxima* nacre pre-treated with sodium hypo chlorate before hydroxyapatite deposition produced a superior coating and could be used for bone tissue engineering. But further in vitro and in vivo studies are needed to validate the biocompatibility and long term stability of this composite coating.

Keywords: Biocompatible, Nano-hydroxyapatite, Oyster shells, Ultrasonic irradiation

INTRODUCTION

The human skeletal system is essential for support and movement of the body. An important structural material forming the skeletal system is an organic-inorganic composite called bone. This natural composite is composed of proteins in the form of collagen fibrils and macromolecules like proteoglycans that are all embedded in a well arrayed inorganic crystalline hydroxyapatite (HAP) matrix.[1,2] It is this remarkable combination and distribution of constituent materials that gives bone its unique mechanical properties and its ability to withstand various mechanical and structural loads encountered during daily physical activity. HAP is a mineral composed of calcium and phosphate ions and has the general formula of $[Ca_{10}(OH)_2(PO_4)_6]$. The close chemical similarity between synthetic HAP and HAP naturally found in bone has led to an extensive research effort focused on using synthetic HAP as a viable bone replacement material in a number of clinical procedures.[3,4] Unfortunately, due to synthetic HAP's low mechanical strength its use has been restricted to low load bearing applications. In a number of cases, its deficiencies have been improved by combining it with other materials. For example, materials such as high density polyethylene and polypropylene have been

successfully combined with synthetic HAP to improve its load bearing capabilities.[5,6] Alternatively, other researchers have gone back to nature to look for a more effective way of producing biosynthetic materials and composites for potential tissue engineering applications. Seashells are naturally occurring ceramic composites that are dense, hard, and remarkably robust. The shell structure has a number of highly desirable mechanical properties that enable it to protect the soft body of the animal against environmental damage and predators. Shells are brittle or quasi-brittle materials composed of mineral components (~95%) and proteins (~5%). It is this compositional blend that gives a shell its high degree of stiffness and hardness. However, shell toughness and its ability to resist crack propagation that has attracted considerable interest.[7,8] This interest stems from the observation that shell fracture toughness can be two to three orders of magnitude greater than the toughness of individual shell components.[9] Another interesting feature is the much larger mechanical strain shells can withstand before failure compared to manmade ceramics.[8,10]

Nacre is the inner iridescent layer found in *Pinctada maxima* (pearl oyster shell) and similar shells such as abalone. Nacre is composed of a crystalline calcium carbonate ($CaCO_3$) mineral phase (aragonite) suspended in an organic matrix. The aragonite is in the form of polygon shaped tablets ranging in size from 5 to 15µm and 0.5 to 1µm in thickness that are stacked into a three dimensional brick wall-like structure. The wall-like structures can consist of columns or sheets depending on the species and typically forms 95% of the composite. Pearl oyster shells have a sheet-like structure. Recent atomic force microscopy studies have shown the individual tablets are suspended in an organic matrix of proteins and polysaccharides that makes up the remaining 5% of the composite.[11,12] Besides the highly advantageous mechanical properties, the nacre is biologically compatible with bone tissues.[13,14] Because of the promising mechanical and biocompatibility properties, nacre is a prime candidate for potential tissue engineering applications. For example, recent animal in vivo studies by Berland et al have shown good cellular interaction between nacre implants and bone forming cells.[15] From another perspective, Vecchio et al have been able to convert *Strombus gigas* (conch) and *Tridacna gigas* (Giant clam) shells to HAP while preserving their original dense columnar structure.[16]

This article reports on the use of synthetically produced HAP and $CaCO_3$ derived from waste oyster shells to form novel HAP/$CaCO_3$ composites and HAP surface coatings on nacre. The first part of the article reports on the crystalline structure and morphology of synthesized nanometre scale HAP powders. The second part examines the use of shell derived $CaCO_3$ that still retains properties of the shell to manufacture HAP/$CaCO_3$ composites. And thirdly, we report on the use of HAP surface coating on nacre substrates to improve biocompatibility and overcome poor mechanical properties inherent with pure HAP constructs.

METHODS

Materials

All chemicals used in this work were supplied by Chem-Supply (Australia) and all aqueous solutions were made using Milli-Q® water (18.3 MΩ cm-1) produced by an ultrapure water system (Barnstead Ultrapure Water System D11931; Thermo Scientific, Dubuque, IA). *Pinctada Maxima* (pearl oyster) shells were supplied raw and were prepared as specified in the following procedure.

Preparation of nanometer scale HAP powders

A detailed description for producing HAP developed by the authors can be found in the literature.[17,18] For completeness, a brief procedural description is outlined as follows.

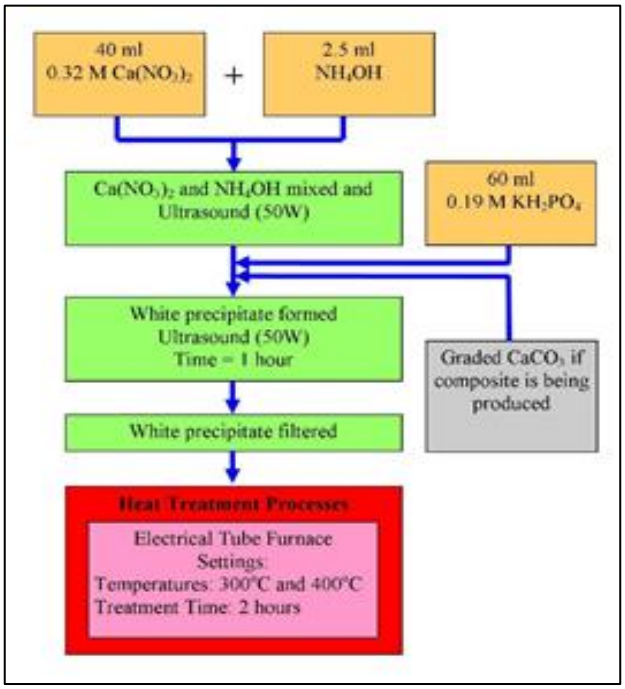

Figure 1: Schematic of synthesis process for producing HAP and HAP/$CaCO_3$ composites.

The procedure begins by first adding a 40mL solution of 0.32 M calcium nitrate tetra-hydrate into a small glass beaker and then adjusting the solution pH to 9.0 using approximately 2.5ml of ammonium hydroxide. The solution is then sonicated using a Hielscher Ultrasound Processor UP50H set at 50 W and maximum amplitude for 1 h. During sonication, 60 mL of 0.19 M potassium di-hydrogen phosphate solution was slowly added while the solution pH was maintained at 9.0 and the Calcium/Phosphate [Ca/P] ratio was maintained at 1.67.

At the end of the sonication period, the solution was centrifuged (15,000 g) for 20 minutes at room temperature to produce a precipitate. The precipitate was collected, washed and centrifuged for a further 10 minutes before being placed into a ceramic boat ready for heat treatment. The heat treatment consisted of placing a sample loaded ceramic boat into an electric tube furnace. The reaction temperatures used were either 300°C or 400°C and the reaction time period was 2 hours for temperatures. After thermal treatment, the agglomerated samples were milled to form an ultrafine HAP powder. A schematic of the synthesis process is presented in (Figure 1).

Preparation of HAP based calcium carbonate composite powders

$CaCO_3$ was derived from *Pinctada maxima* (pearl oyster) shells. The shells were first washed and scrubbed to removal all traces of organic matter. This was followed by giving the shells a final wash down using Milli-Q® water and then allowing them to air dry before being stored for the next stage of process. Shell material was used in two forms. In the first form shells underwent milling to produce $CaCO_3$ powders of varying grades. A metallurgical ring crusher was used to crush and grind the shells into a powder. After grinding, a Roto-Tap was used for 30 minute to sieve the powder. Sieving produce a variety of powder grades ranging from 38 to 850 micrometres as seen in (Figure 2). In the second form shells were cut into 1 cm^2 test substrates.

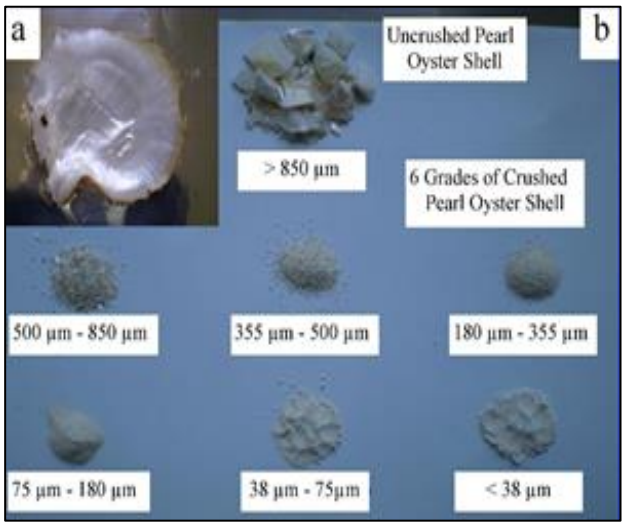

Figure 2: (a) *Pinctada maxima* (pearl oyster) shells and (b) Various grades produced after sieving $CaCO_3$ powder (38 to 850 micrometers).

Preparation of the HAP/$CaCO_3$ composites started by selecting the appropriate $CaCO_3$ grade and then weighing out the required mass. In this case the mass percentages of $CaCO_3$ selected were 5% and 10%, with the remaining mass balance made up of HAP powder. However, before being incorporated into the HAP synthesis process the $CaCO_3$ powders were bleached for 30 minutes. The bleached $CaCO_3$ was then added to the HAP processing procedure to produce the required blend as seen in (Figure 1). Visual inspection during processing and after heat treatment revealed a noticeable difference between pure HAP powders, pure $CaCO_3$ powders and the respective HAP/$CaCO_3$ powder blends. However, differences between the 5% and 10% $CaCO_3$ blends were much harder to distinguish and could only be differentiated under electron microscopy. (Figure 3) presents a representative image of a 10% $CaCO_3$ blend.

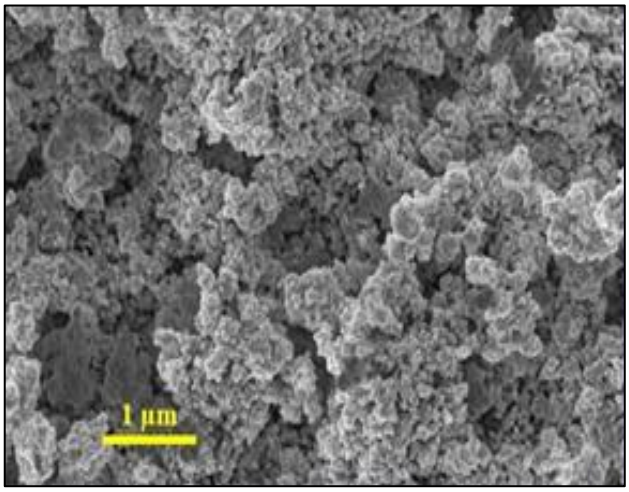

Figure 3: Representative electron microscopy image of HAP/$CaCO_3$ powder blend.

Preparation of shell substrates

The second part of the study used the shell as a substrate for the deposition of a HAP coating. The substrates were prepared by first pre-washing and cleaning the raw shells. After cleaning the shells were placed in a clean bench vice and cut into 1 cm^2 test substrates using a standard hacksaw (32 teeth per 25mm). Substrates were then washed in running water in the lab sink to remove all cutting debris. In the next stage of cleaning samples were placed into a 250ml beaker of Milli-Q® water then exposed to ultrasonic irradiation for 10 minutes to remove any loose particles that may have been embedded in the samples during the cutting stage. After the first irradiation, the Milli-Q® water was changed and the process repeated. In total, the samples were treated three times before being air dried and stored ready for surface treatment.

Substrate surface treatments and coatings

A specific surface pre-treatment was applied to each respective substrate prior to coating. This was done to gauge the effectiveness of each surface pre-treatment in promoting coating attachment. Five pre-treatment procedures and an untreated substrate (control) were investigated and details of each pre-treatment are presented in (Table 1). The surface coating procedure

consisted of using a spatula to evenly spread a layer of HAP powder over the surface of sample types 2 to 6, sample 1 being the unloaded control sample. After coating, all samples were placed into ceramic furnace boats and then individually placed into a pre-heated furnace set to 400°C. Samples remained in the furnace for 2 hours to calcify the coating in the presence of atmospheric air. After 2 hours of thermal treatment, the ceramic boats were removed from the furnace and allowed to cool down to room temperature in air.

Table 1: Substrate surface pre-treatments used prior to coating application.

Substrate type	Surface treatment	Description
1	None (Control)	Sample is cleaned using Milli-Q® water and then air dried.
2	Chemical Hydrochloric Acid (HCl)	Sample is placed into a 500ml beaker containing 200ml of Milli-Q® water and 10 ml of 35% HCL. Solution pH was measured and found to be 1. The sample remains in the solution for 3 minutes. It is then removed and washed with Milli-Q® water and air dried.
3	Chemical Sodium Hypo Chlorate (SH)	Sample is placed into a 500ml beaker containing 200ml of household bleach. (45g/l of sodium hypo chlorate). The sample remains in the solution for 30 minutes. It is then removed and washed with Milli-Q® water and then air dried.
4	Boiling (B)	Sample is placed into a 500ml beaker containing 200ml of Milli-Q® water and boiled for 10 minutes. It was then removed and washed with Milli-Q® water and then air dried.
5	Mechanical Abrasion (A)	Sample is roughened using silicon carbide sand paper (180p). 15 lateral movements followed by 15 vertical movements. The sample was then placed into a 500ml beaker containing 200ml of Milli-Q® water and exposed to 5 minutes of ultrasonic irradiation to remove any loose particles and contamination from the sand paper. The sample was then air dried.
6	Mechanical (S)	Sample is placed into a bench vice. The sample is scored by 20 lateral movements (both directions) by a surgical scalpel. The sample was then placed into a 500ml beaker containing 200ml of Milli-Q® water and exposed to 5 minutes of ultrasonic irradiation to remove any loose particles. The sample was then air dried.

Advanced characterization

Powder X-ray diffraction (XRD) spectroscopy was used to identify the crystalline size and phases present in synthesized HAP powders. Spectroscopy data was recorded at room temperature, using a Siemens D500 series diffractometer [Cu Kα=1.5406Å radiation source] operating at 40kV and 30mA. The diffraction patterns were collected over a 2θ range of 20° to 60° with an incremental step size of 0.04° using flat plane geometry with a 2 second acquisition time for each scan. The crystalline size of the particles was calculated using the Debye-Scherrer equation (Equation 1) from the respective spectroscopy patterns. Field emission scanning electron microscopy (FESEM) was also used to study size, shape and morphological features of the various powders. All micrographs were taken using a high resolution FESEM [Zeiss 1555 VP-FESEM] at 3kV with a 30µm aperture operating under a pressure of 1.333×10^{-10} mbar. Samples were mounted on individual substrate holders using carbon adhesive tape before being sputter coated with a 2nm layer of gold to prevent charge build up using a Cressington 208HR High Resolution Sputter coater.

RESULTS

XRD spectroscopy analysis of synthesised HAP powders

XRD spectroscopy was used to identify the crystalline size of the synthesised nanometre scale HAP powders. A representative XRD pattern of a thermally treated HAP powder (400ºC for 2 h) is presented in (Figure 4). The pattern shows the main (h k l) indices found in the sample, namely (002), (211), (112), (300), (202), (310), (222), (213) and (004). These indices match the known phases present in pure HAP and are consistent with the phases listed in the ICDD database. The crystalline size, $t_{(hkl)}$, of each sample was calculated from the respective XRD patterns using the Debye-Scherrer equation below.[19-20]

$$t_{(hkl)} = \frac{0.9\lambda}{B\cos\theta_{(hkl)}} \quad (1)$$

where, λ is the wavelength of the monochromatic X-ray beam, *B* is the full width at half maximum (FWHM) of the peak at the maximum intensity, $\theta_{(hkl)}$ is the peak diffraction angle that satisfies Bragg's law for the (h k l) plane and $t_{(hkl)}$ is the crystallite size. The crystallite size of each sample was calculated from the (002) reflection peak. HAP samples thermally treated at 400ºC gave a mean particle size of 30 nm.

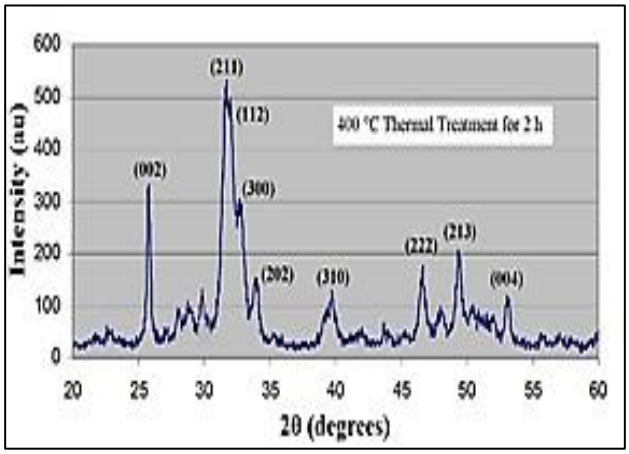

Figure 4: Representative XRD pattern of a HAP powder after thermal treatment.

FESEM analysis of pure and blended powders

FESEM was used to study particle size and morphology of the pure powders and blended powders. Representative micrographs of manufactured powders are presented in (Figure 5). (Figure 5b) reveals a spherical/granular particle morphology that is highly agglomerated and is typical of the synthesised HAP powder samples. Also present in (Figure 5b) are three 50 nm diameter circles placed randomly to highlight the spherical/granular morphology. This morphology is similar to particle morphologies previously reported in the literature.[21-22]

The raw $CaCO_3$ powder was sifted through a 38 micron sieve to produce a relatively homogeneous powder consisting of thin plates and finer granular shaped particles ranging in size from 20 to 100nm as seen in (Figure 5a). A representative micrograph of a HAP/$CaCO_3$ composite (5%) is presented in (Figure 5c) and reveals the presence of granular shaped particles with pronounced edges that appear to be moderately packed and range in size from 50 to 100nm. This is in stark contrast to the smooth and spherical HAP particle morphologies seen in (Figure 5b). (Figure 5d) presents a representative micrograph of a HAP/$CaCO_3$ (10%) and also reveals the presence of tightly packed granular particles. The particles range in size from 50 to 100nm and have similar morphology to particles seen in the HAP/$CaCO_3$ (5%) composite. Analysis of FESEM micrographs taken of composite samples has confirmed the influence of $CaCO_3$ on particle morphology during the synthesis of the HAP composites. Furthermore, investigation of the various surface pre-treatments and coatings revealed varying degrees of effectiveness in coating the substrates and these results are evaluated in the following discussion section.

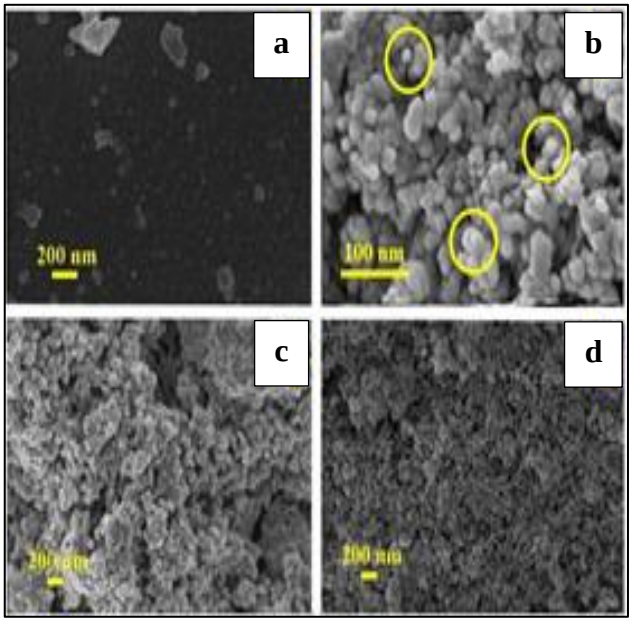

Figure 5: (a) Milled $CaCO_3$ powder sifted through a 38 micron sieve; (b) Pure ultrafine HAP powder; (c) HAP/$CaCO_3$ composite (5% $CaCO_3$ and particle sizes less than 38 micron) and (d) HAP/$CaCO_3$ composite (10% $CaCO_3$ particle graded between 38 and 75 microns).

DISCUSSION

The HAP powders synthesised in the present work had structural and chemical properties similar to those reported in the literature.[23,24] XRD analysis also confirmed the crystallinity of the sample powders were similar to those reported by other researchers and in particular conformed well to previous crystal structure modelling carried out by the authors.[25,26] The spherical/granular morphology of the nanometre scale HAP particles was also consistent with those produced by similar ultrasound based synthesis techniques.[27,28] The manufactured HAP powders also displayed similar physiochemical properties to those manufactured using other techniques such as wet precipitation and spray pyrolysis.[29,30] In terms of HAP based coating techniques, the present work used a straightforward treatment technique that did not require complex and expensive application equipment or complex processes such as ion beam surface structuring, plasma-vapour and surface patterning and texturing.[31] HAP deposition and coating attachment on the various substrate types used in the present work revealed some interesting surface features after thermal treatment. After thermal treatment in a conventional tube furnace each substrate showed some degree of lamellae bubbling. Inspection of the Type 1 (control-no surface pre-treatments) substrate revealed

signs of surface bubbling, but still retained its pearlescent lustre. The remaining 5 substrate types all exhibited a dull white coating that indicated HAP had indeed adhered to the respective surfaces. The appearance of this type of deposition is consistent with similar HAP deposition studies.[32,33] The Type 2 (HCl) substrate also showed signs of minor delaminating, but the majority of the HAP coating remained attached to the surface. While the Type 3 (SH) substrate that had undergone a bleaching pre-treatment showed the most significant change. Its surface had a very distinctive white appearance that was much thicker and denser when compared to the other substrate types. The Type 4 (B) substrate which had undergone a boiling pre-treatment showed significant lamellae delaminating. The substrate was also found to be very brittle after the thermal treatment. Overall, the Type 4 substrate displayed poor mechanical properties and inferior surface properties compared to the other substrate types. Studies by other researchers have shown the importance of good mechanical compliance for ceramic coating to be effectively used in any tissue engineering application.[34] The present work has shown the Type 4 substrate is unsuitable for tissue engineering applications. On the other hand, both Type 5 (A) and Type 6 (S) substrates revealed significant amounts of HAP was trapped within the rough surface features created by the respective surface texturing treatments. Surface texturing used in Type 6 trapped the largest amounts of HAP and significantly contributed to coating integrity. Generally, both surface texturing techniques were found to be beneficial in promoting surface fixation of the coatings. Studies have shown that texturing of implant surfaces can improve protein adsorption and promote positive cellular responses.[35] However, in the present case further cell-line studies are needed to confirm the biocompatibility and suitability of the substrates.

FESEM surface studies carried out on the various substrate types also revealed some interesting surface features. Interestingly, the Type 1 (control) substrate was found to have traces of HAP on its surface, even though there was no HAP coating was applied to its surface. The presence of individual HAP particles was found to be the result of ongoing calcification processes occurring within the furnace environment as seen in (Figure 6a). During thermal treatment, both water and NH_4 evaporating from surrounding substrates tended to deposit on everything within the furnace, including the Type 1 substrate. However, the other substrate types did not show this type of surface feature. Examining the FESEM images of the Type 2 (HCI) substrate revealed a thick surface covering, unfortunately the coating was not uniformly distributed over the entire surface. Numerous uncoated regions could be seen over the substrates surface, which revealed the underlying lamellae structure as seen (Figure 6b). The poor surface covering makes the Type 2 an inferior substrate and tends to reduce the coating functionality and biological response ability to various cell-line.[36] Type 3 (SH) substrates were evenly covered with a thick and dense HAP surface coating and unlike the Type 2 substrate had far fewer exposed underlining lamellae regions. The deposited HAP produced a superior coating on the pre-treated (bleached) surfaces of Type 3 substrates than those of the acid pre-treated (HCI) surfaces of the Type 2 substrates as seen in (Figure 6c) and (Figure 6d). In both cases, the mean HAP particle size found on both substrate types was estimated to be around 500 nm. In the case of Type 5 and Type 6 substrates, the surface coatings were not thick or uniformly distributed. Instead the HAP tended to accumulate within and around the roughened (textured) surface features. This type of deposition resulted in poor surface coverage and produced large areas of uncoated substrate. However, further studies are needed to fully investigate the effects of surface texturing, and in particular the effects of surface texturing before chemically treating substrates with bleach as in the case of Type 3 substrates. The pre-treated (bleaching) Type 3 (SH) substrates were found to produce a superior HAP surface coating compared to other substrate types tested in this study. Future studies are planned to investigate the wear properties and load bearing capacity of the Type 3 (SH) substrates. In addition, in vitro studies are also planned to investigate the biocompatibility of the substrates towards a number of bone cell-lines.

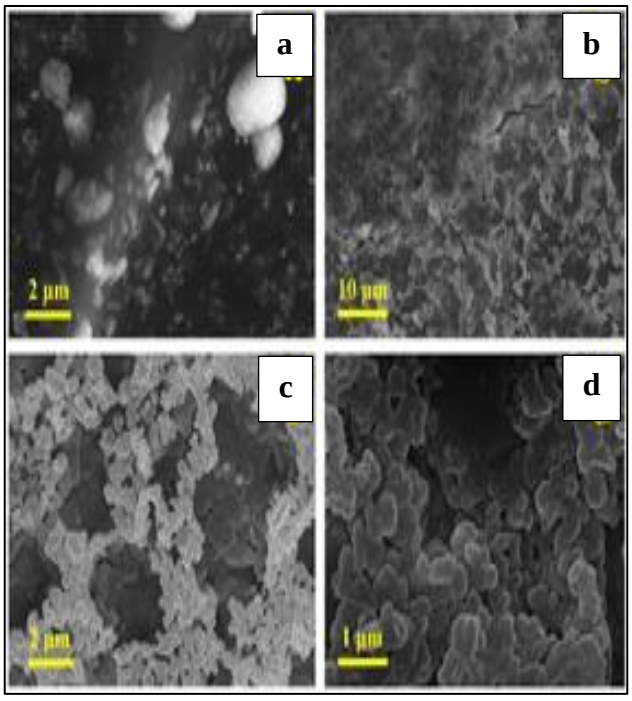

Figure 6 FESEM analysis of various substrate surfaces: (a) Substrate Type 1 (Control) showing the deposition of HAP particles during the calcination process; (b) Type 2 (HCl) showing minor delaminating of the thin HAP coating; (c) Type 2 (HCl) enlarged view of coating with underlying lamellae exposed, and (d) Type 3 (SH) substrate showing an evenly distributed thick coating over the entire substrate surface with far fewer exposed lamellae regions.

CONCLUSION

HAP is a calcium phosphate that is considered to be a viable replacement for bone material in a number of low-load bearing tissue engineering applications. While the nacre layer found inside the *Pinctada maxima* (pearl oyster) shell is hard, stiff, and extremely tough. The present study has shown that a nanometer scale HAP powder (mean particle size of 30 nm) can be combined with sieved powders derived from *Pinctada maxima* ($CaCO_3$) to produce a composite powder. During synthesis, the addition of sieved powders were found to influence particle size and morphology of composite powders. The tough nacre was used as a substrate and a number of surface pre-treatments were investigated before the substrates were coated with HAP. The results of the investigation revealed a substrate pre-treated with sodium hypo chlorate (Type 3) before HAP deposition produced the superior coating. The surface coating was thick, dense and evenly distributed. However, further studies are needed to investigate wear properties and load bearing capacities of the Type 3 substrate. Future in vitro studies are planned to determine the biocompatibility of the substrates towards a number of bone cell lines.

ACKNOWLEDGEMENTS

Authors would like to thank Dr. Xuan Le for her assistance with FESEM analysis.

Funding: No funding sources
Conflict of interest: None declared
Ethical approval: The study was approved by the Institutional Ethics Committee

REFERENCES

1. Weiner S, Wagner HD. The material bone: structure-mechanical function relations. Ann Rev Mater Sci. 1998;28:271-98.
2. Hellmich C, Ulm FJ. Average hydroxyapatite concentration is uniform in the extracollagenous ultrasturture of mineralized tissues: evidence at the 1-10µm scale. Biomechan Model Mechanobiol. 2003;2:21-36.
3. Habraken WJEM, Wolke JGC, Jansen JA. Ceramic composites as matrices and scaffolds for drug delivery in tissue engineering. Adv Drug Deliv Rev. 2007;59:234-48.
4. Hutmacher DW, Schantz JT, Lam CXF, Tan KC, Lim TC. State of the art and future directions of scaffold-based bone engineering from a biomaterials perspective. J Tissue Eng Regen Med. 2007;1:245-60.
5. Bonner M, Ward IM. Hydroxyapatite/polypropylene composite: A novel bone substitute material. J Mater Sci Letters. 2001;20(22):2049-51.
6. Ono I, Tateshita T, Nakajima T. Evaluation of a high density polyethylene fixing system for hydroxyapatite ceramic implants. Biomaterials. 2000;21:143-51.
7. Currey JD. Mechanical properties of mother of pearl in tension. Proc R Soc. 1977;196:443-63.
8. Barthelat F. Nacre from mollusk shells: a model for high-performance structural materials. Bioinsp Biomim. 2010;5(035001):1-8.
9. Wegst UGK, Ashby MF. The mechanical efficiency of natural materials. Phil Mag. 2004;84:2167-81.
10. Kamat S, Su X, Ballarini R, Heuer AH. Structural basis for the fracture toughness of the shell of the conch Strombus gigas. Nature. 2000;405:1036-40.
11. Rousseau M, Lopez E, Stemfle P, Brendie M, Franke L, Guette A, et al. Multi-scale structure of sheet nacre. Biomaterials. 2005;26:6254-62.
12. Li XD, Chang WC, Chao YJ, Wang RZ, Chang M. Nanoscale structural and mechanical characterization of a natural nanocomposite material: the shell of red abalone. Nano Lett. 2004;4:613-7.
13. Lamghari M, Almeida MJ, Berland S, Huet H, Laurent A, Milet C, et al. Stimulation of bone marrow cells and bone formation by nacre: in vivo and in vitro studies. Bone. 1999;25:91-4.
14. Pereira-Mouries L, Almeida MJ, Milet C, Berland S, Lopez E. Bioactivity of nacre water-soluble organic matrix from the bivalve mollusk *Pinctada maxima* in three mammalian cell types: fibroblasts, bone marrow stromal cells and osteoblasts. Comp Biochem Physiol B. 2002;132:217-29.
15. Berland S, Delattre O, Borzeix S, Catonne Y, Lopez E. Nacre/bone interface changes in durable nacre endosseous implants in sheep. Biomaterials. 2005;26:2767-73.
16. Vecchio KS, Zhang X, Massie JB, Wang M, Kim CW. Conversion of bulk seashells to biocompatible hydroxyapatite for bone implants. Acta Biomaterialia. 2007;3:910-8.
17. Poinern GEJ, Brundavanam R, Le X, Djordjevic S, Prokic M, Fawcett D. Thermal and ultrasonic influence in the formation of nanometre scale hydroxyapatite bio-ceramic. Int J Nanomed. 2011;6:2083-95.
18. Poinern GEJ, Brundavanam R, Le X, Nicholls PK, Cake MA, Fawcett D. The synthesis, characterisation and in vivo study of a bioceramic for potential tissue regeneration applications. Sci Rep. 2014;4(6235):1-9.
19. Klug HP, Alexander LE. X-ray diffraction procedures for poly-crystallite and amorphous materials. 2nd ed. New York, Wiley; 1974.
20. Barrett CS, Cohen JB, Faber J, Jenkins JR, Leyden DE, Russ JC, et al. Advances in X-ray analysis. New York: Plenum Press; 1986:29.
21. Han Y, Li S, Wang X, Bauer I, Yin M. Sonochemical preparation of hydroxyapatite nanoparticles stabilized by glycosaminoglycans. Ultrasonics Sonochem. 2007;14(3):286-90.
22. Zhuo ZH, Zhou PL, Yang SP, Yu XB, Yang LZ. Controllable synthesis of hydroxyapatite

nanocrystals via a dendrimer-assisted hydrothermal process. Mater Res Bull. 2007;42(9):1611-8.
23. Elliott JC. Structure and chemistry of the apatite's and other calcium Orthophosphates. Amsterdam: Elsevier; 1994.
24. Eanes ED. Amorphous calcium phosphate. Monogram, Oral Sci. 2001;18:130-47.
25. Kumta PN, Sfeir C, Lee DH, Olton D, Choi D. Nanostructured calcium phosphates for biomedical applications: novel synthesis and characterization, Acta Biomater. 2005;1:65-83.
26. Brundavanam RK, Poinern GEJ, Fawcett D. modelling the crystal structure of a 30nm sized particle based hydroxyapatite powder synthesised under the influence of ultrasound irradiation from x-ray powder diffraction data. Am J Mater Sci. 2013;3(4):84-90.
27. Poinern GEJ, Brundavanam RK, Mondinos N, Jiang ZT. Synthesis and characterisation of nanohydroxyapatite using an ultrasound assisted method. Ultrasonic Sonochem. 2009;16:469-74.
28. Poinern GEJ, Brundavanam RK, Le X, Djordjevic S, Prokic M, Fawcett D. Thermal and ultrasonic influence in the formation of nanometer scale hydroxyapatite bio-ceramic. Int J Nanomed. 2011;6:2083-95.
29. Santos MH, Oliveira M, de Freitas PL, Mansur HS, Vasconcelos WL. Synthesis control and characterisation of hydroxyapatite prepared by wet precipitation process. Mater Res. 2004;7:625-30.
30. An GH, Wang HJ, Kim BH, Jeong YG, Choa YH. Fabrication and characterization of a hydroxyapatite nanopowder by ultrasonic spray pyrolysis with salt-assisted decomposition. Mater Sci Eng A. 2007;821:449-51.
31. Ramakrishna S, Ramalingam M, Kumar STS, Soboyejo WO. Biomaterials: A nano approach. Boca Raton, FL: CRC Press; 2010.
32. Shi D, Jiang G., Synthesis of hydroxyapatite films on porous Al_2O_3 substrate for hard tissue prosthetics. Mater Sci Eng. 1998;6:175-82.
33. Campbell AA. Bioceramics for implant coatings. Mater Today. 2003;6:26-30.
34. Best SM, Porter AE, Thian ES. Bioceramics: Past, present and for the future. J Euro Ceram Soc. 2008;28:1319-27.
35. Le X, Poinern GEJ, Ali S, Berry CM, Fawcett D. Engineering a biocompatible scaffold with either micrometre or nanometre scale surface topography for promoting protein adsorption and cellular response. Int J Biomater. 2013;782549:1-16.
36. Rabiei A, Blalock T, Thomas B, Cuomo J, Yang Y, Ong J. Microstructure, mechanical properties, and biological response to functionally graded HA coatings. Mater Sci Eng C. 2007;27:529-33.

Cite this article as: Brundavanam RK, Fawcett D, Poinern GEJ. Synthesis of a bone like composite material derived from waste pearl oyster shells for potential bone tissue bioengineering applications. Int J Res Med Sci 2017;5:2454-61.